UNIVERSITAT POLITÈCNICA DE CATALUNYA
BARCELONATECH
Escola Tècnica Superior d'Enginyeria
de Telecomunicació de Barcelona

NUMERICAL ANALYSIS OF A SPHERICAL SENSING STRUCTURE FOR 3D HEAT FLOW & WIND SENSING

A Master's Thesis

Submitted to the Faculty of the

Escola Tècnica d'Enginyeria de Telecomunicació de Barcelona

Universitat Politècnica de Catalunya

by

UYGAR ATALAY

In partial fulfilment

of the requirements for the degree of

MASTER IN ENGINEERING PHYSICS

Advisor: MANUEL DOMINGUEZ- PUMAR

Barcelona, November 2020

Title of the thesis: Numerical Analysis of a Spherical Sensing Structure For 3D Heat Flow & Wind Sensing

Author: Uygar Atalay

Advisor: Manuel Dominguez-Pumar

Abstract

This thesis presents a series of numerical analysis of a novel spherical sensing structure for 3D heat flow and wind sensing. Unique spherical structure of the sensor made it possible to use it both for aboveground and underground. First, buried sensor setup is simulated and the effect of covering film & thermal resistance between sensors are investigated. Then, atmospheric sensor setup is simulated and the thermal impedance is investigated. The sensor is promising to offer detailed information of a local thermal environment for the planetary bodies or for further explorations on small bodies.

Acknowledgements

Thanks to Manuel Dominguez for the supervision and the advice during this thesis.

Revision history and approval record

Revision	Date	Purpose
0	07/11/2020	Document creation
1	09/11/2020	Document revision

Written by:		Reviewed and approved by:	
Date	07/11/2020	Date	09/11/2020
Name	Uygar Atalay	Name	Manuel Dominguez-Pumar
Position	Project Author	Position	Project Supervisor

Table of contents

List of Figures

1. Introduction

Measuring the wind speed and direction on the surface of a body is a key success in planetary exploration. This success has caught great attention for the first time when Mars rover Curiosity has landed in 2012. The atmosphere of Mars is composed of 95% carbon dioxide with a pressure nearly 1% of the one in Earth. Temperature of the atmosphere range from 150 K to 300 K. In these extreme circumstances, sensors using dynamic pressure does not properly work. So, best option here becomes thermal anemometry technique.

On the other hand, it is relevant to mention the concept of heat flux. Heat flux is a measure of thermal energy transfer and it is a fundamental parameter used in many engineering and research applications. Its transfer mechanisms are conduction, convection and radiation. To measure the heat flux; thermophiles, infrared radiation, calorimetry, etc., technics can be used.

As space exploration gains speed exponentially, one promising area of heat flux measurement shows itself in planetary exploration. The key information heat flux offers here, is about geophysical processes. By measuring this phenomenon, energy balance on the surface and subsurface of the planet can be studied. The diurnal, seasonal and also annual temperature variations of the surface are linked strongly to the thermal properties of the subsurface, which is just a few centimetres deep. Thus, the heat flow quantified in this very shallow surface region, can provide a detailed understanding of the heat transfer mechanisms occurring in these temperature cycles.

The parameters effecting temperature change depend on the grain size, densification of the regolith and the interactions between regolith and the atmosphere. These interactions may be caused by any gas adsorption inwards regolith, or desorption outwards regolith.

The measurement of heat flux under planetary regolith may even create an opportunity to obtain planetary heat flux, if the depth of measurement does not allow any annual or diurnal temperature cycles to be noticed. This may tell us more about the thermal history of a planetary body.

This thesis study is about a wind speed and direction sensor designed for the atmosphere of Mars. The sensor is structured on a spherical shell, which is divided into four triangular sectors. The sectors are individually controlled to have a constant temperature above and independent of the ambient one.

It is designed & fabricated in UPC and is relatively a promising new technique of wind sensing. Components of the sensor is shown below:

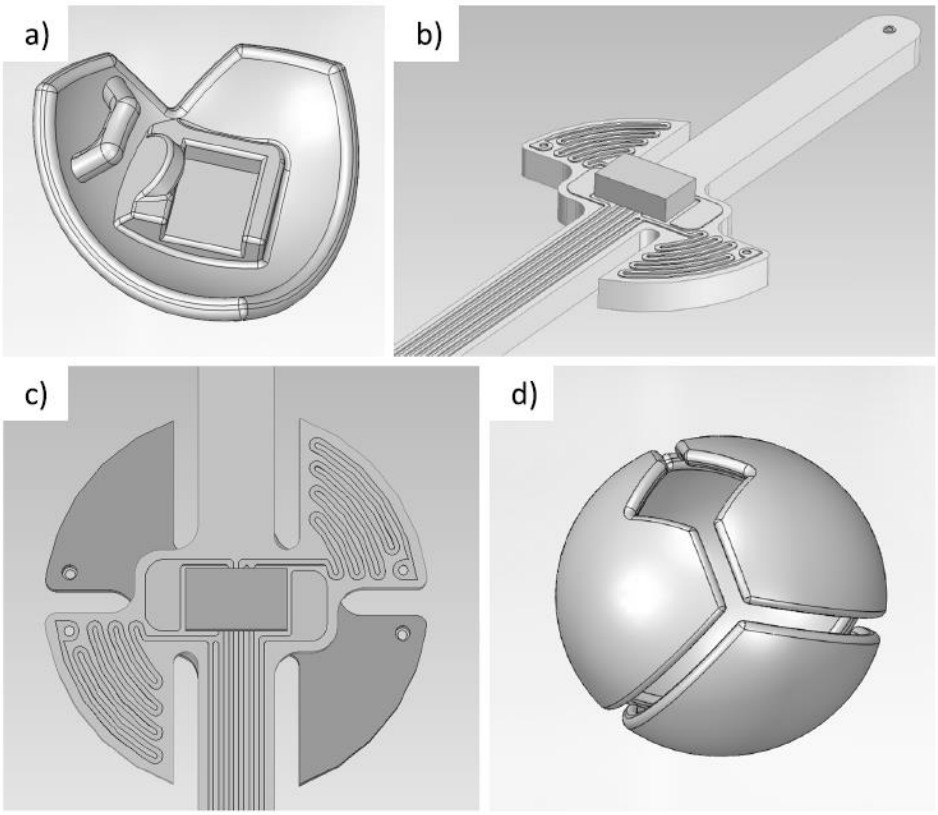

Figure 1. Models of the new wind sensor components: a) Triangular sector with its interior heat resistor mold. b) Printed circuit board with electrical instalment & core resistor. c) assembly of two printed circuit boards. d) Assembly of four sectors creating a spherical structure. [1]

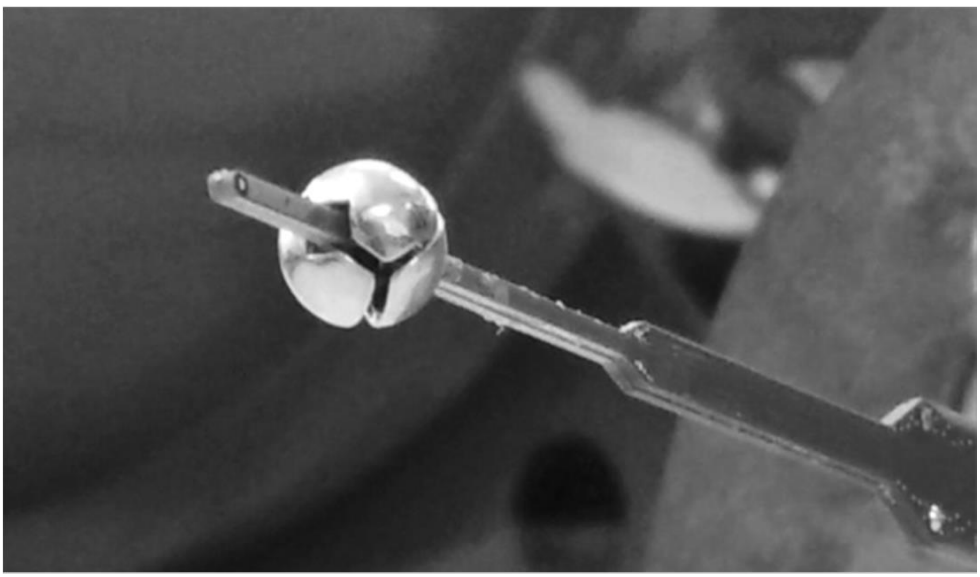

Figure 2. A prototype of the spherical wind sensor [1]

There are also some advantages of the spherical structure of the sensor when compared to other wind sensing techniques. They can be listed as following:

- Its shape provides an axisymmetric & a flow which is laminar
- It provides minimal sector number with maximum efficiency
- The resistors are protected from outside by the spherical sectors
- The heat dissipated from the supporting structure via conduction is minimized
- Thermal model needed for simulations is simplified as there is only one temperature value, which is the constant temperature of the sectors

The study which is carried on here is a continuation of calculations and simulations or further new try-outs of this new wind sensor. Above the innovative technique the sensor offers for wind sensing, it can also make a breakthrough in characterization of heat transfer in regolith of planets & planetary bodies.

By burying the sensor underground, it can provide information on instantaneous local thermal environment surrounding a rover or lander, which makes it probably the first sensor capable of measuring local 3D heat flux.

At the beginning of the thesis, it is planned to make experiments in person individually in the laboratory where experiment setup stays. Just when the laboratory environment is familiarized, access to the university is blocked. Due to this disastrous situation COVID-19 pandemic created, studies had to be continued via computer environment and any physical experiments are blocked. Thus, objectives are fixed amid the thesis period.

The objectives of this thesis can be divided into two; first part being about the heat transfer in regolith and the second part, being about the heat transfer in carbon dioxide atmosphere:

1.
    1.1. To understand the effect of the plastic film coverage, which is protecting the sensor from outside regolith and dust, to heat flux dissipating from the sensor
    1.2. To calculate the thermal resistance between the sectors of 3D heat flux sensor
2.
    2.1. To perform calculations of the thermal impedance of 3D heat flux sensor.

2. State of the art of the technology used or applied in this thesis

The history of wind sensing is as old as 1976, when Viking sent the first measurements of wind on the surface of Mars. It was based on thin cylinders covered by platinum resistors. 2 decades later, Pathfinder improved this with a heated platinum-iridium wired thermal wind sensor. Currently, Curiosity includes two "bolt-like" booms on the rover's mast ("neck"), heated by platinum resistors and sends current data to Earth. This structure is in a tool called REMS (Rover Environmental Monitoring Station).

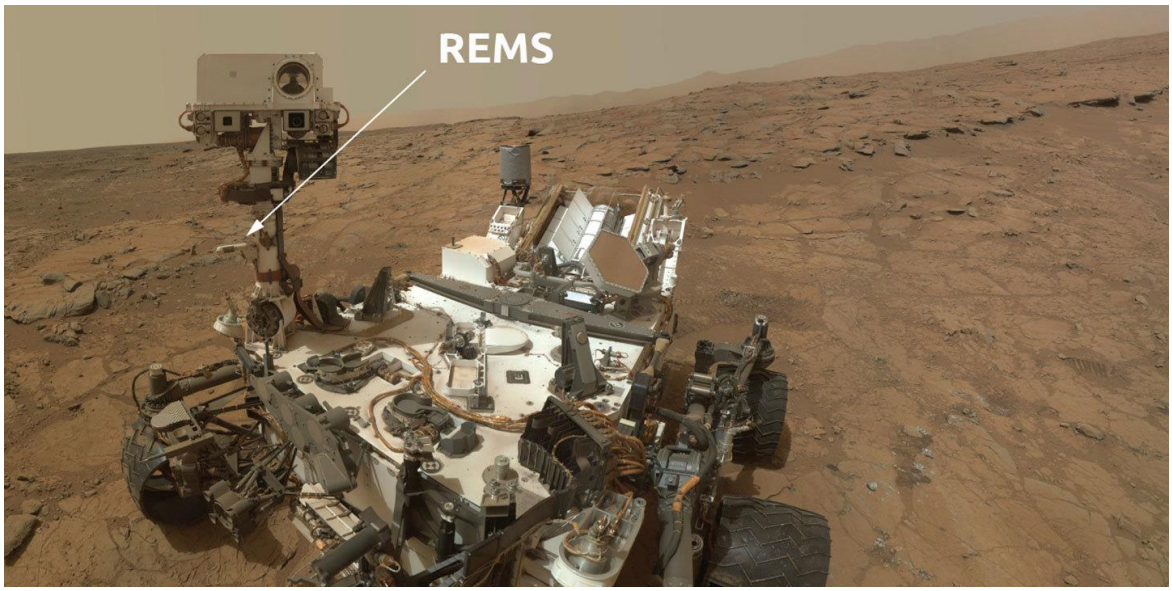

Figure 3. A selfie from the Mars Curiosity Rover, showing the location of REMS. [2]

Then, with a paper published in IEEE Sensors Journal in 2016, an innovative novel wind speed and direction sensor is introduced. This sensor was developed in UPC (Universitat Politecnica de Catalunya), with the contribution to the project MEIGA (Mars Environmental Instrumentation for Ground and Atmosphere). It was basically a heritage of the REMS Curiosity wind sensor. Taking this sensor as a fundament, radical changes applied and the sensor evolved to a radically improved version. Spherical design of the sensor made the measurements more versatile and precise. The challenges were about power and mass restrictions beside the desired interaction wind interaction area and also the obligation to protect the inside area of the sensor. These challenges are successfully eliminated with this innovative design change. The simulation & experiment results were promising that it is even decided to use the sensor for planetary regolith.

This thesis is grounded on this above-mentioned paper and the sensor introduced in this paper. Prosecution of simulations is aimed for both wind sensing and its usage under regolith. Therefore, most resources were dependent on this paper and the research conducted around this paper.

However, for one objective, it was required to look from a different perspective. This objective was the thermal impedance calculations. As the term ‘impedance’ is originally an electric related term, the challenge here was to change the electrical domain to thermal domain.

In order to find the relation parameters, a literature review had to be made. The inflictor was about ‘frequency’ parameter. It is inherent for electrical engineering, but it is difficult to find its twin for thermal domains. This literature review was mainly on understanding how to change domains.

Apart from that, simulation software and MATLAB codes were already present and ready to use with small lacks. This led to a quick start for implementations without need for comprehensive literature review.

3. Methodology

This chapter includes all relevant methods that have been used. It is divided into four parts respectively; the aims of this thesis, what research methods are used, how are those research methods are used and how the relevant analysis is made & consistent results are obtained.

3.1. Aims

This project is consisted of more than one research questions. These questions can be listed as following:

1. What level of impact does the plastic film covering the sensor, which is put to protect it from regolith, have on the heat flux from the sensor?
2. What is the relation between thermal conductivity of the regolith, thermal conductivity the plastic film and the heat dissipated from the sensor?
3. What is the relation between thermal resistance between sensor sectors and thermal resistivity of the regolith?
4. What is the relation between thermal impedance of the sensor and thermal frequency?
5. What is the relation between phase difference of temperature & heat flux functions and thermal frequency?

3.2. Research Methods

These main problems of this project are dealt by collecting data from various software which were MATLAB and COMSOL Multiphysics® Modeling Software. All data are gathered by designing experimental setup and executing simulations by controlling various variables.

For the first problem, a MATLAB code and a COMSOL file which are previously prepared for this kind of simulations is used. An addition of a plastic layer is defined by myself for COMSOL and this simulation setup output is used in MATLAB to get the final results, which is the power signals from the sensor.

For the second problem, only COMSOL simulation outputs are needed. To be able to change the thermal conductivity of the plastic layer in a huge range with small step sizes, continuous simulations had to be done consecutively. This problem is solved by using a parameter sweep extension in COMSOL. With this add-in, large amount of data is obtained and used to execute overall graphs.

Third research problem is required to have its own experimental design, because thermal resistance calculations were a new study topic in this project. COMSOL platform is again used for these designs. Analysis part is also done with graphs.

Fourth question is the enhancement of the previous one. The previous design is improved and sensor design is approximated to the original experimental setup with its sectors' real allocations.

The final research problem is different than the previous ones. While first four problems dealt with the heat transfer in regolith underground, final one dealt with the heat transfer in a flowing gaseous environment, which was carbon dioxide. Thus, experiment setup is again changed in COMSOL and required data are obtained & analysed afterwards.

3.3. Explanation of the Research Methods Chosen

First studies of plastic film calculations began with a previously designed COMSOL document and a previously coded MATLAB file. The aim of the MATLAB file was to generate power signals of sectors by virtually rotating the sensor. Output was directly showing maximum power generated from sectors. On the other hand, the aim of the COMSOL file was to simulate sensor setup, to build a real-life demonstration for the real setup. However, it was not fully completed. Some fixing and small improvements had to be done.

Plastic coverage of the sensor is originally 5-10 um thickness, but because of the mesh size issues, thickness of the plastic is selected as 1 mm. The minimum thickness without any trouble is identified as 0.72 mm. Instability rose below this value.

For this case, four variables are changed using parameter sweep tool inside COMSOL:

- Temperature difference between top and bottom is adjusted to obtain a certain heat flux
- Thermal conductivity of the regolith
- Thermal conductivity of the plastic film
- Dimensions of the regolith medium

It is necessary to include here that side walls of the regolith body are insulated while top, bottom and sphere temperatures are held constant.

An example of the software used for this section is shown below.

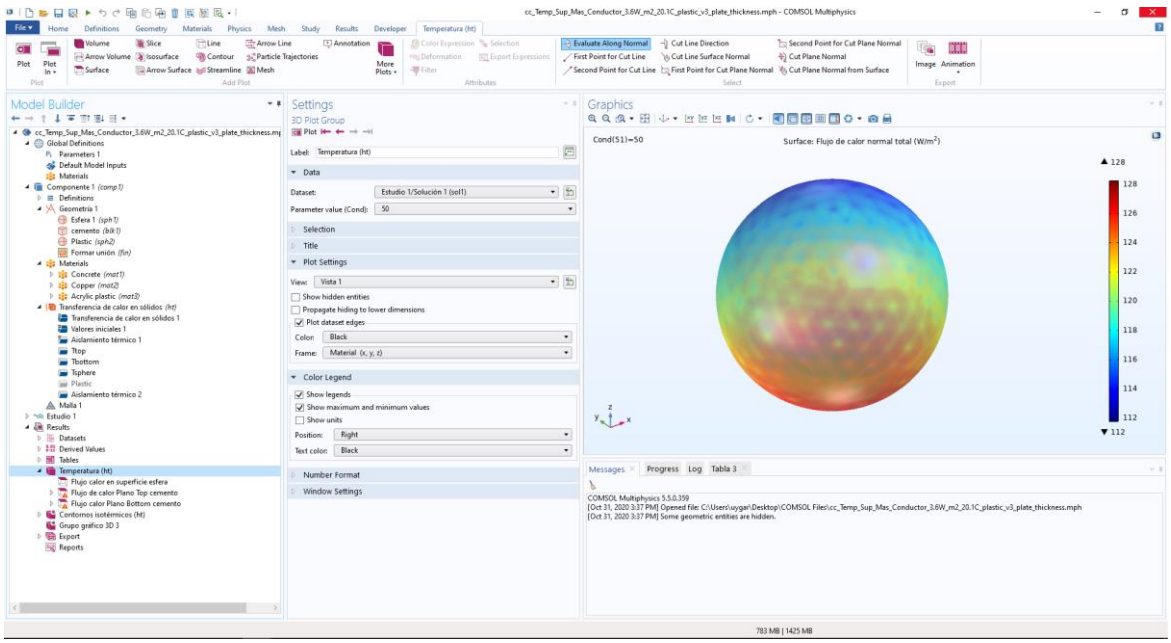

Figure 4. An example screen shot from the COMSOL software, used for this part of the study.

After a redesign process, third question is investigated only by manipulating regolith's thermal conductivity value, as plastic film is no more used. Inside surface of the sectors and the side walls are insulated, while top, bottom and outside sectors parts are held at a constant temperature.

For the penultimate and final cases, since the medium is changed from regolith to carbon dioxide, manipulated variables became the thermal frequency and the wind speed.

In this part of COMSOL simulation, Multiphysics tool is used. Heat transfer in fluids and laminar flow approaches are combined. Boundary conditions are set as the cylindrical pipe had insulated side wall, while top & bottom of the cylinder was at constant temperature. Atmospheric pressure was also at a constant value. The inlet wind speed is manipulated to see the effect of it to thermal impedance and phase difference, while temperature of the sphere is changed according to a sinusoidal function specified prior to the simulation.

3.4. Analysis

Obtained data for all parts of the study is whether analysed by MATLAB or Excel. For the first research question, power signal graphs are acquired via MATLAB. Again, MATLAB is used for the measurements for the phase differences in the last part of the study. One weakness for the last approach was measuring the angle differences between functions manually. This issue could be dealt by founding an automated way to measure, however,

time required to solve this problem would be inefficient when compared to manual measurement.

Data preparation for analysis is also an important procedure, but data acquired from COMSOL were compatible with MATLAB or Excel as the output were matrixes.

4. Results

The results chapter is divided into two parts; first one presenting calculations for the sensor buried under regolith, and the second one presenting calculations on thermal impedance for the sensor in a CO_2 -flowing wind tunnel.

4.1. Calculations Over Sensor Protection Film & Thermal Resistance of the 3D Heat Flux Sensor

4.1.1. Simulating the Effect of the Plastic Film over the Heat Flux Sensor

MATLAB files which are meant to simulate four different sectors of the heat transfer sensor are used to calculate the power signals in the sensor with respect to a change in angle. The aim of the files is to calculate the heat flux for each sector and iterate this for every angle indicating a full rotation of the sensor in its own axis.

Figure 5 shows the heat flux integrated over each of the 4 sectors as a function of the yaw angle for a pitch angle of 45º, for an incoming heat flux of 3.6 W/m^2. Amplitude of the signals is proportional to the incoming heat flux. The thermal conductivity of the regolith here is 0.9 W/mK. Temperatures for top and bottom sources are 20.1°C and 19.9°C respectively. Temperature of the sphere is taken as 21°C.

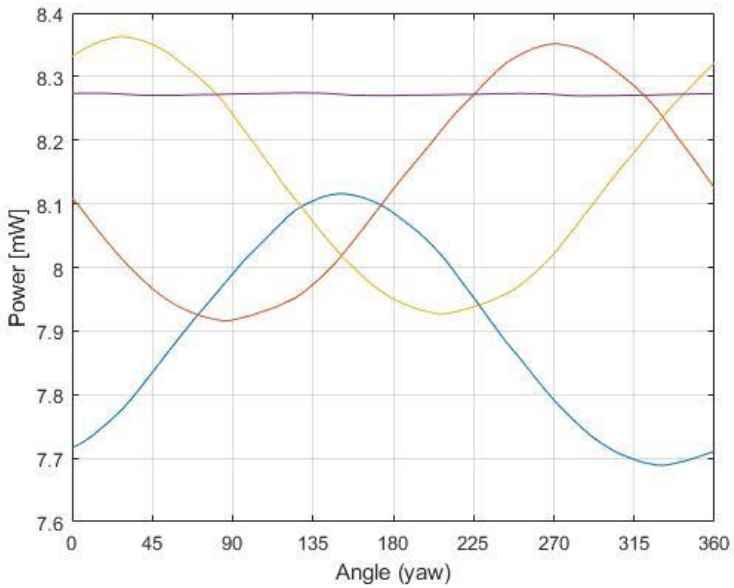

Figure 5. Simulated power signals in the sensor. Two apparent sectors can be identified here: Rotation directed sector has constant power signal as its heat flux does not change with the angle. Sector that has the lower power signal band is closer to the hotter part of the system as it dissipates less heat to the environment.

It is easier to compare power changes when each sector data is subtracted from its mean value, which provides a clear cut. Figure 6 shows this version of the graph.

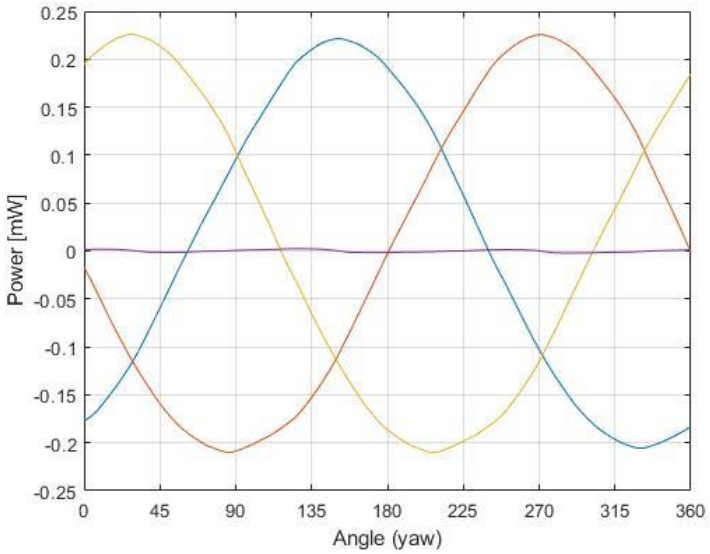

Figure 6. Power signals in the sensor with regard to the average.

A combined power output for two different incoming heat fluxes is shown in Figure 7. Dotted lines are for 3.6 W/m^2 and continuous lines are for 7.2 W/m^2. To obtain the heat flux of 7.2 W/m^2, temperatures of the top & bottom plates are adjusted to 20.05°C and 19.95°C respectively.

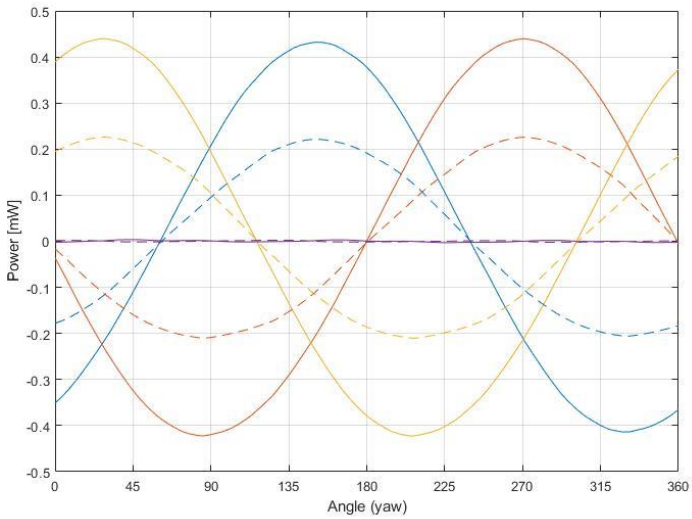

Figure 7. Simulated power signals in the sensor. Comparison of heat fluxes, 3.6 W/m^2 (dotted lines) and 7.2 W/m^2 (continuous lines) where the regolith conductivity is 0.9 W/mK

Figure 8 shows the same simulation for a regolith conductivity of 1.8 W/mK. The results are almost identical indicating that constant temperature operation generates signals truly dependent on heat flow and not only on temperature gradient.

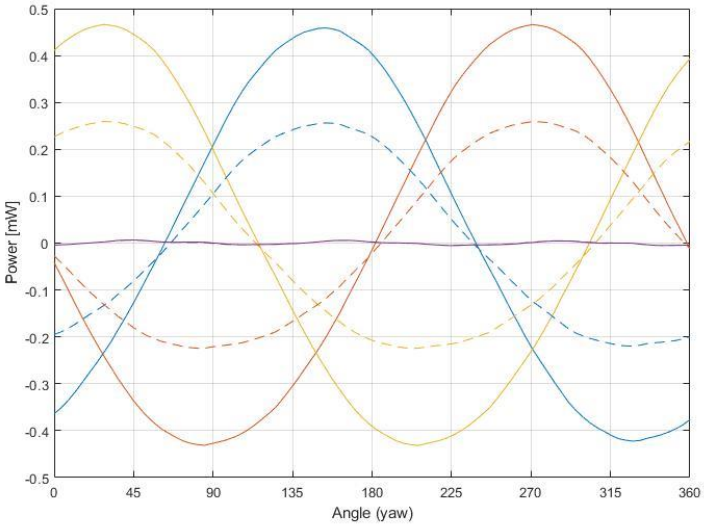

Figure 8. Simulated power signals in the sensor which is identical to Figure 7. Only difference is the regolith's thermal conductivity which is 1.8 W/mK in this case.

Physical world is for sure hard to predict. Our sensor is covered by a thin plastic film package in order to prevent any sand to enter inside and create any trouble under the ground. Therefore, the effect of this thin plastic layer to the heat transfer from the sphere sensor must be investigated.

A plastic coverage layer of 1 mm is added just on the sphere in COMSOL software. Selected material is a prebuilt-plastic under the software and it has a thermal conductivity of 0.18 W/mK.

Figure 7 and Figure 8 can be drawn again, considering this plastic layer. Figure 9 and Figure 10 show the power signals of the sensor, containing an extra plastic layer outside.

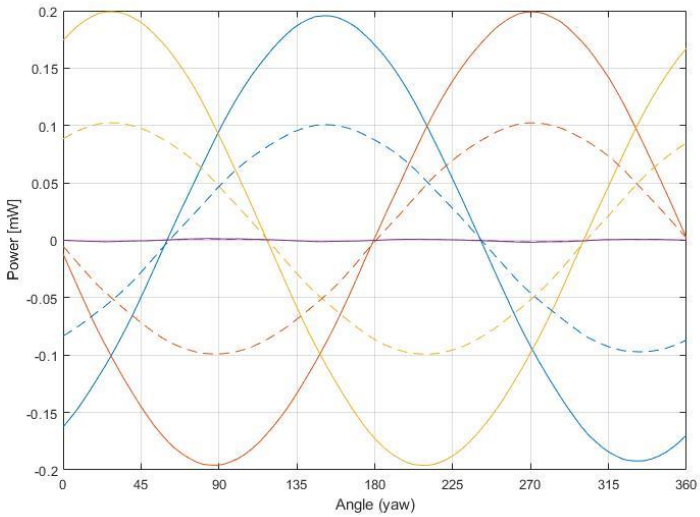

Figure 9. Simulated power signals in the sensor. Comparison of heat fluxes; 3.6 W/m^2 (dotted lines) and 7.2 W/m^2 (continuous lines) where the regolith conductivity is 0.9 W/mK with an additional plastic coverage of 1 mm.

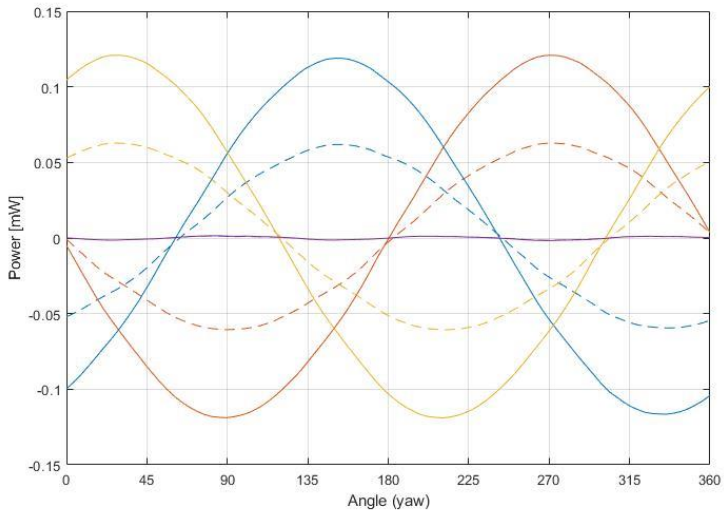

Figure 10. Simulated power signals in the sensor. Comparison of heat fluxes; 3.6 W/m^2 (dotted lines) and 7.2 W/m^2 (continuous lines) where the regolith conductivity is 1.8 W/mK with an additional plastic coverage of 1 mm.

The effect of plastic film seems large enough to notice. An added film decreased the dissipated heat from the sensor.

These simulation results can be crosschecked by changing the thermal conductivity of plastic to that of the cement which is the material of the surrounding.

Figure 11 and Figure 12 shows the power signals in the sensor where the material of the extra layer is changed to cement. These graphs in principle are identical with Figure 7 and Figure 8 respectively.

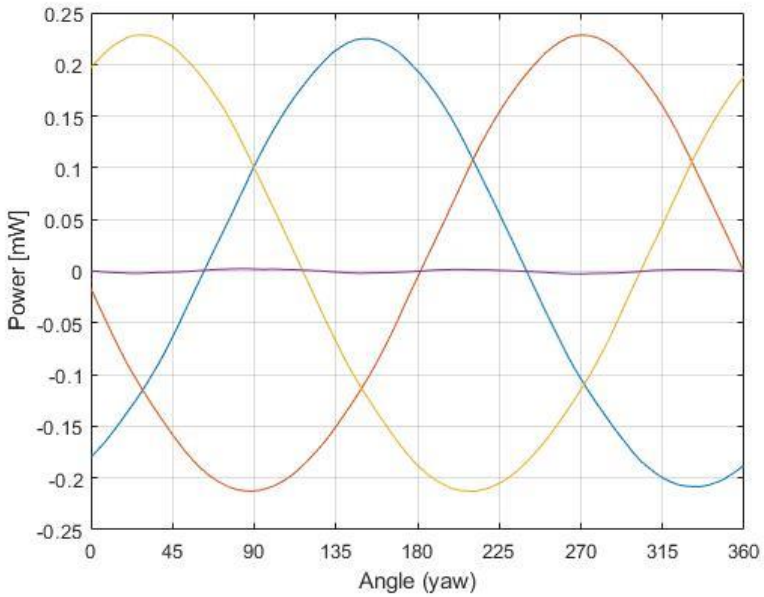

Figure 11. Simulated power signals in the sensor for the heat flux of 3.6 W/m^2, which is identical with Figure 7.

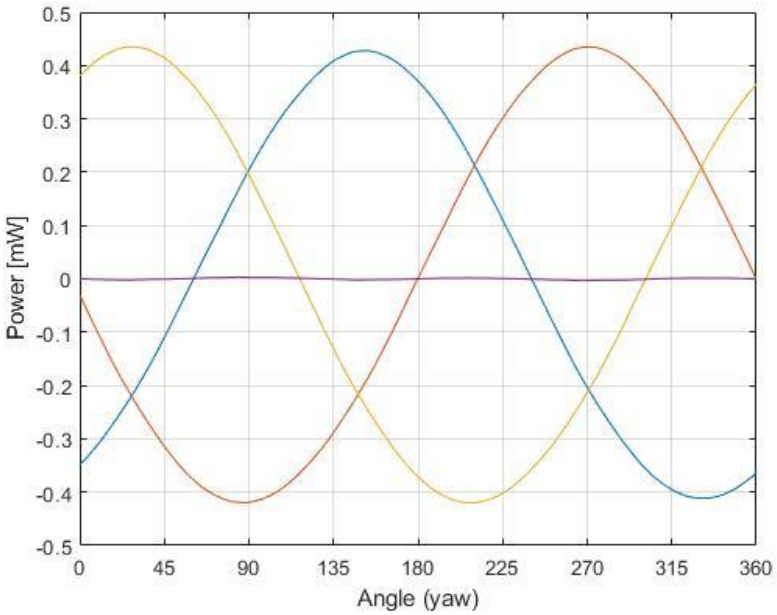

Figure 12. Simulated power signals in the sensor for the heat flux of 7.2 W/m^2, which is identical with Figure 8**.**

It can be seen with ease that the previous simulations are correct as they are crosschecked above.

At this point, it is convenient to decrease the thickness of the plastic layer as the thickness used in the above simulations is 1 mm which is quite thick. Desired thickness should be in the range of 50-100 um.

Unfortunately, mesh size at this level creates an unstable state and makes it harder to get a proper solution. Minimum thickness without any unstable situation is obtained as 0.72 mm. Below of this thickness created unpredictable results.

A solution here is found to be adjusting the thermal conductivity of the plastic layer, so that the effect would be the same as there was a change in thickness. In other words, a raised thermal conductivity has the same effect as a lowered thickness.

A stable plastic film thickness of 1 mm is used for this case. By also providing the plastic thermal conductivity in the range of 0 to 5.5 W/mK, power signal for every step can be seen. The only distinct property of these power waves is their amplitude. A power signal wave indicates a plus and minus maximum power. The absolute value of this, is important to be used.

Figure 13 below shows the maximum absolute values of power signals as a function of plastic's thermal conductivity. Various regolith conductivities are used to see the effect of the environment.

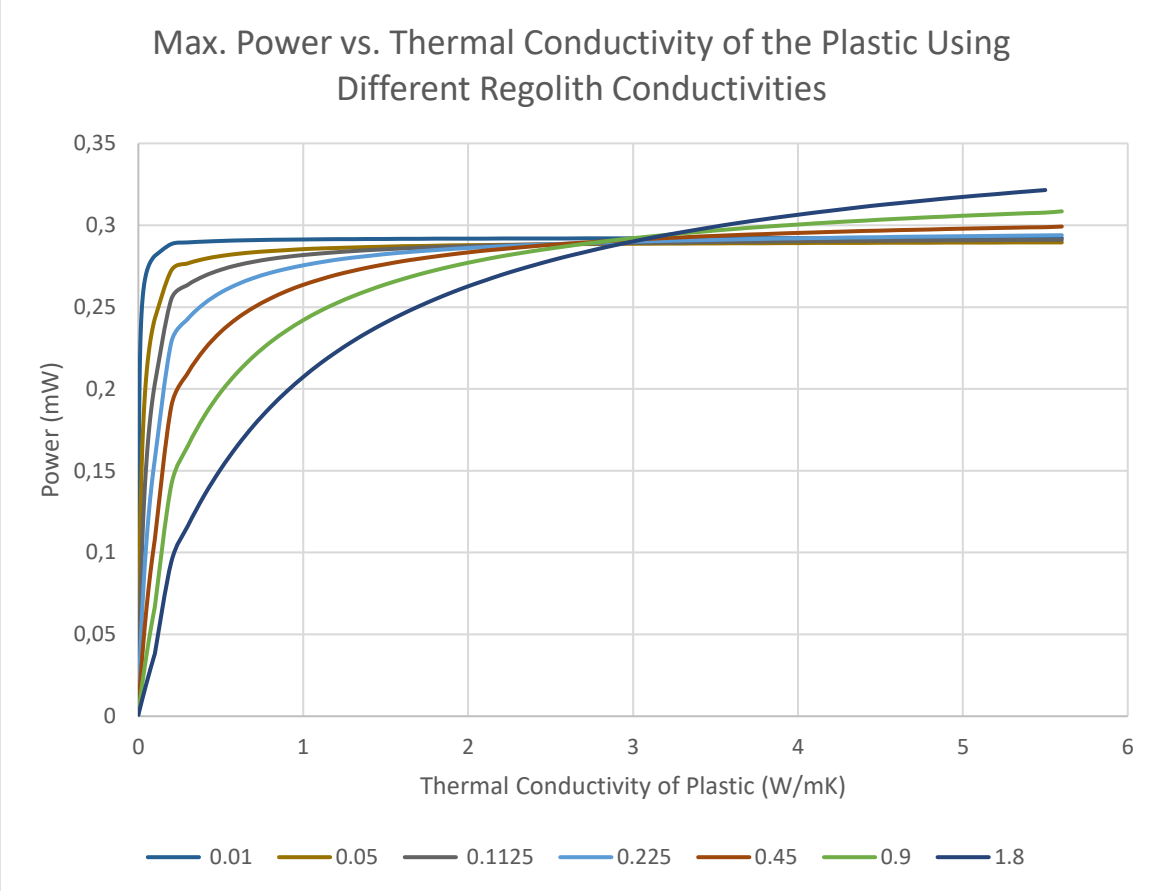

Figure 13. Maximum absolute power amplitude values as a function of the thermal conductivity of plastic film. Different lines are obtained by using seven different regolith thermal conductivities. One can see that when regolith becomes less conductive, the line becomes edgy. On the contrary, when regolith becomes highly conductive, lines become rounder.

Herein, it is uncertain to see if all lines converge at some further point. In order to see this, an extension on x-axis should be made to higher values of plastic's thermal conductivity.

Figure 14 shows the same simulation with more data points and an extension of the x-axis values to 50 W/mK.

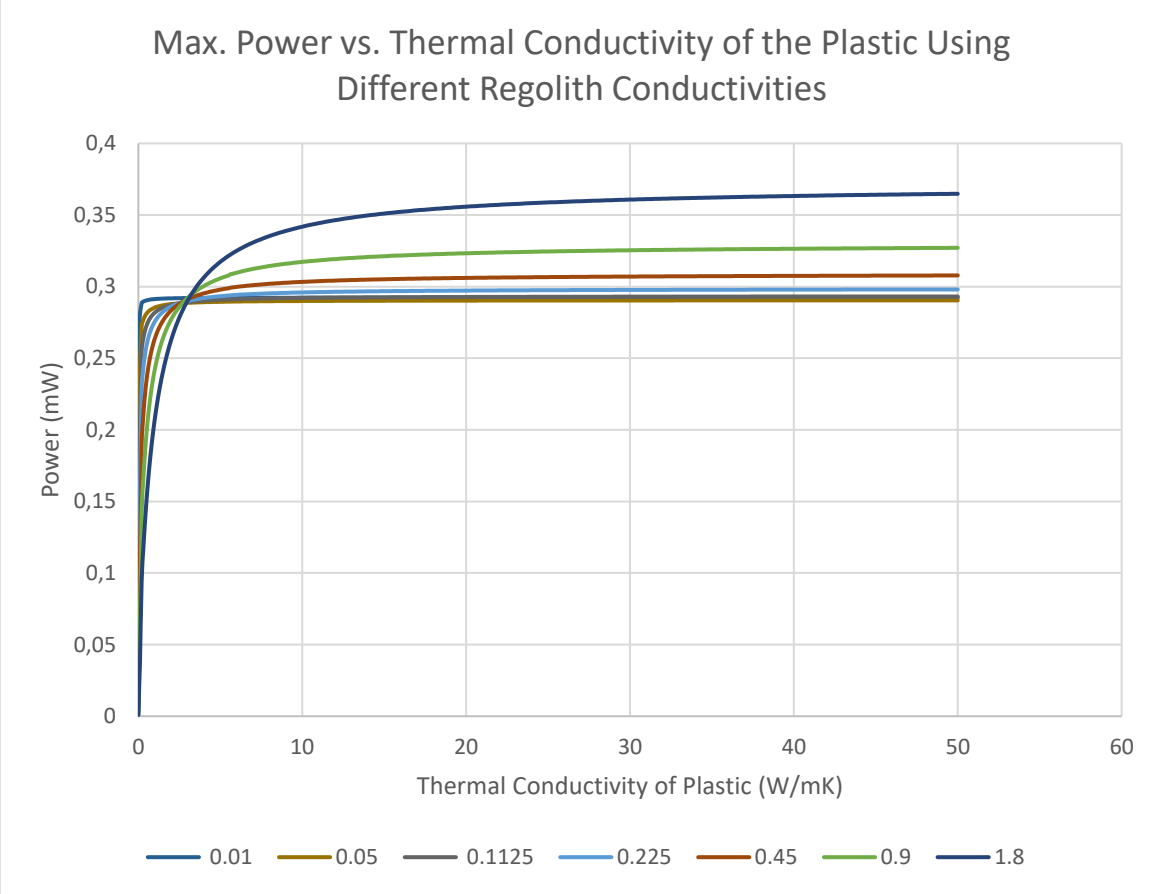

Figure 14. Same simulation path as shown in Figure 13, with addition of more data points in the extended region of 0 to 50 W/mK thermal conductivity of plastic.

It can be assumed that all maximum power values would eventually meet at a certain power amplitude value at the y-axis.

If this does not the case, perhaps boundary conditions are meagre. To make boundary conditions more accurate and to keep out their unwanted effects, it is better to enlarge the size of regolith body.

Different body heights are tested and it is seen that further the sensor away from top and bottom sides, lower the amplitude of the power signal becomes. This also means that the heat dissipating from the surface of the sensor becomes more homogeneous throughout top & bottom sides.

Figure 15 shows the effect of regolith body height to the amplitude of the power signal from the sensor.

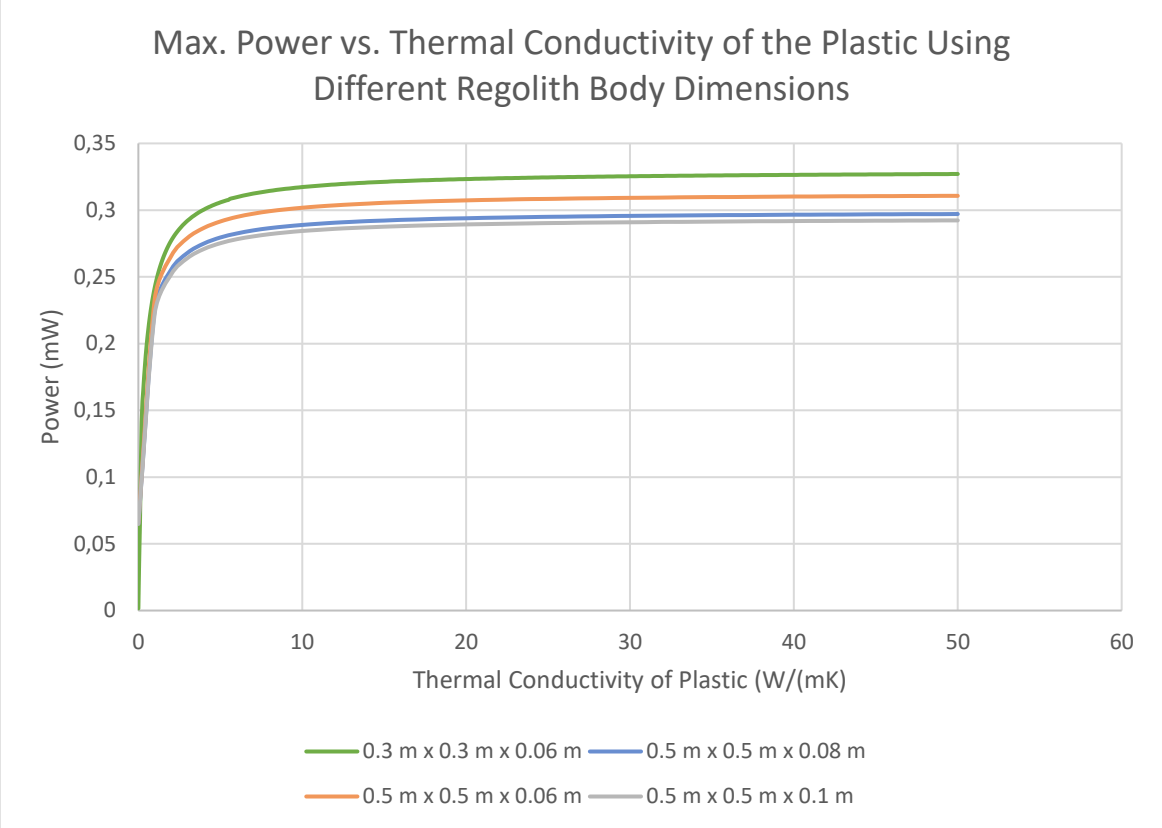

Figure 15. Impact of the regolith body height to the amplitude of the power signal from the sensor. The thermal conductivity of the regolith here is selected as 0.9 W/mK

Enlargement tests continued to find a proper dimension value for sides. After some more tests, it is decided that the most stable size of the body is 0.5 m x 0.5 m x 0.10 m instead of the original size of 0.3 m x 0.3 m x 0.06 m. In these margins, graphs for different plastic thermal conductivity values converged each other, pointing out a rough average power amplitude value.

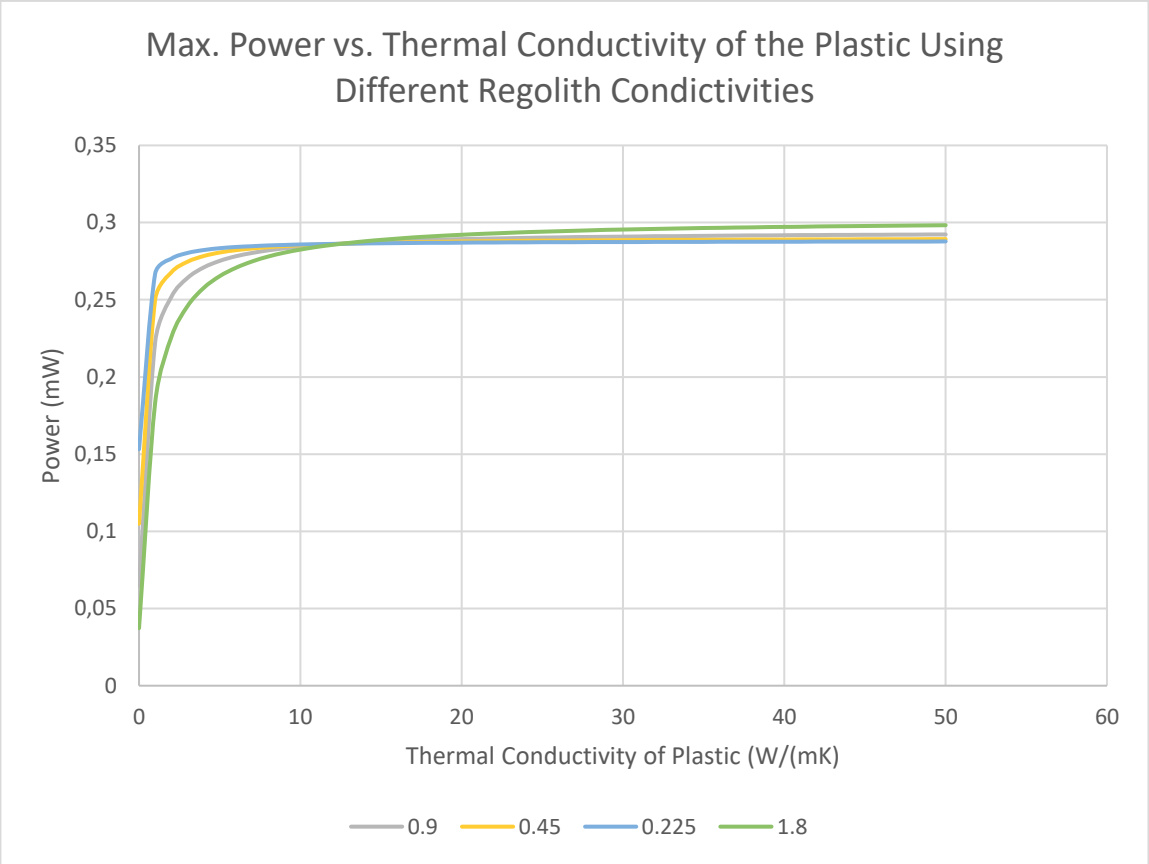

Figure 16. Maximum absolute power amplitude values as a function of the thermal conductivity of plastic film. Enlargement of the regolith body to 0.5 m x 0.5 m x 0.10 m made the solution clearer. Despite using four different regolith conductivities, all lines seem to converge near 0.3 mW.

Also, power values for no plastic film are like the following:

Regolith Conductivity (W/mK)	Max. Power (mW)
1,8	0,2504
0,9	0,2285
0,45	0,2175
0,225	0,212
0,1125	0,2092
0,05	0,2077

Table 1. Power Values for No Use of the Plastic Film

These data point out a slight increase in the maximum power value when the regolith's thermal conductivity is increased.

4.1.2. Calculations for the Thermal Resistance between Sensor Sectors

Two sequent targets are decided for this part: First one is to design a sphere sensor body having two separate sectors, and the second one is to design a four-sector sensor body where sectors are located in exact positions as in the real-life original one.

4.1.2.1. Thermal Resistance Calculations for Two Sectors

In order to avoid any mesh size issues, thickness of the sectors is selected as 1 mm and the distance between sectors is selected as also 1 mm. Material which fills the inside gap of the sensor is selected as air from COMSOL preloaded materials. Temperature difference between desired sectors is selected as 1 K to obtain direct results. With these inputs thermal resistance between sectors becomes as following:

$$Thermal\ Resistance\ Between\ Sectors = \frac{21\ °C - 20\ °C}{Total\ Normal\ Heat\ Flux\ for\ Sector_1 - Total\ Normal\ Heat\ Flux\ for\ Sector_2}$$

Figure 17. Total normal heat flux through surface in W/m^2. Due to low temperature on bottom, lower regions of sector dissipate more heat, indicating higher normal heat flux.

Enormous heat flux values are seen on the edges, where heat dissipates quicker due to the corner shape of the structure.

Following pictures show the temperature distribution in the regolith body from different axis' and perspectives:

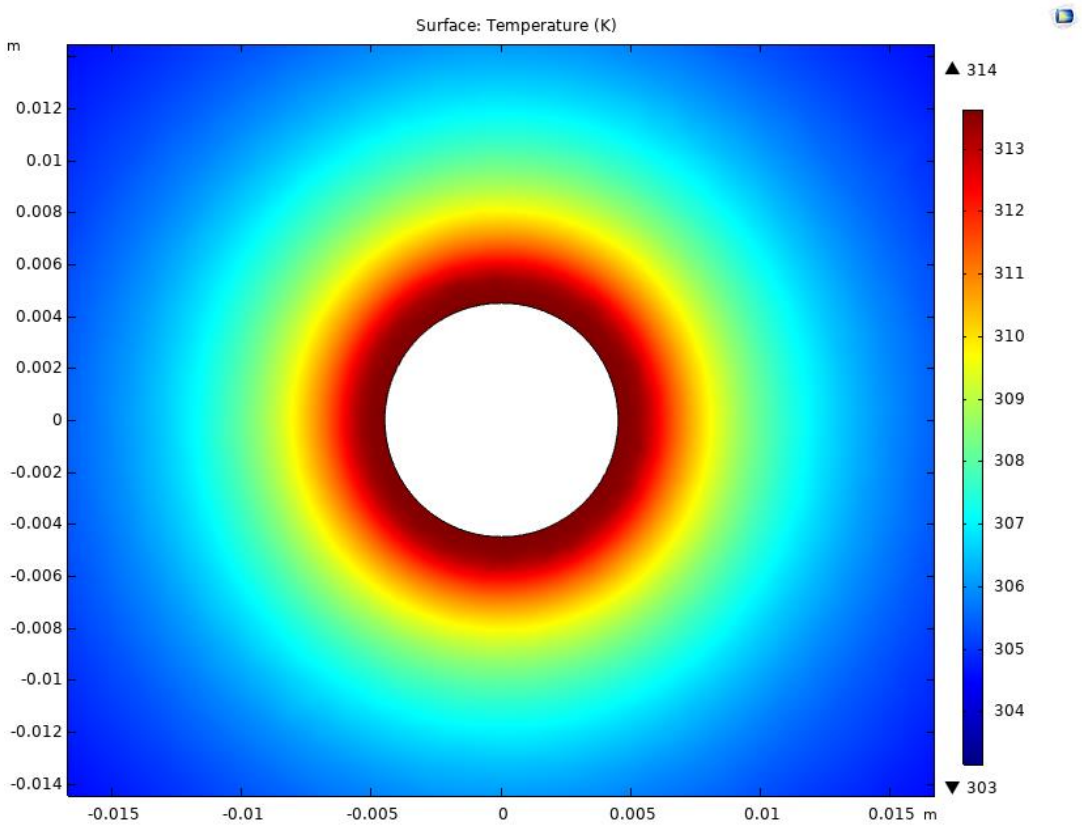

Figure 18. Temperature distribution in the regolith, excluding sensor body. The axis here is the horizontal axis as no difference is observed between two sectors.

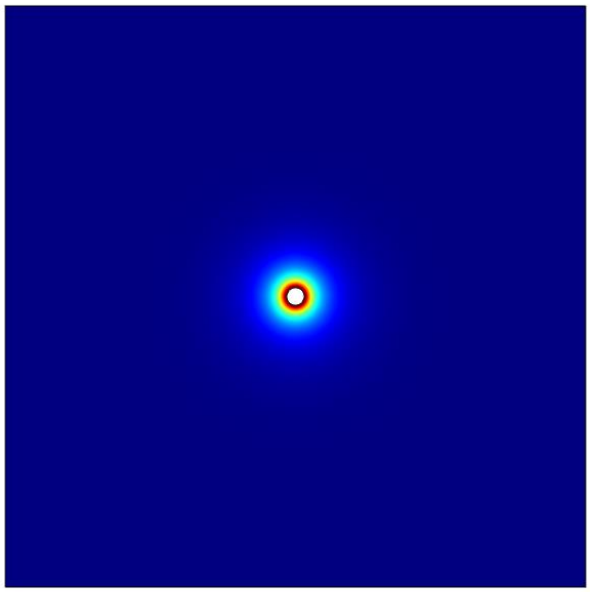

Figure 19. The same perspective as Figure 18 but a thorough look to the complete setup.

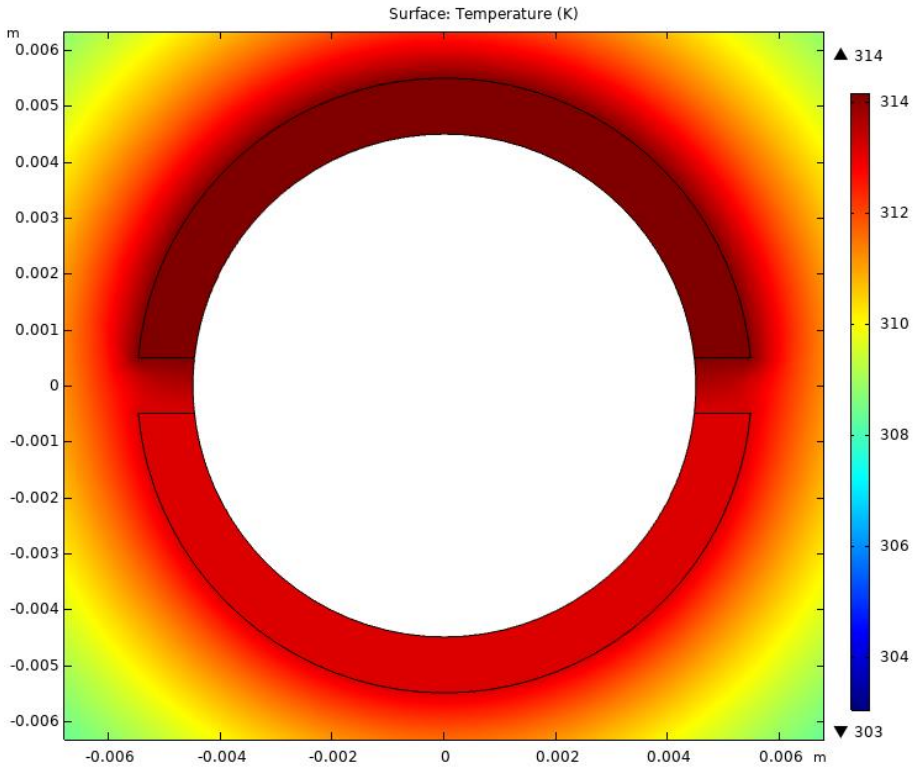

Figure 20. Temperature distribution between sectors from a vertical angle, excluding the inside volume of the sensor. 1 K temperature difference between sectors can easily be seen.

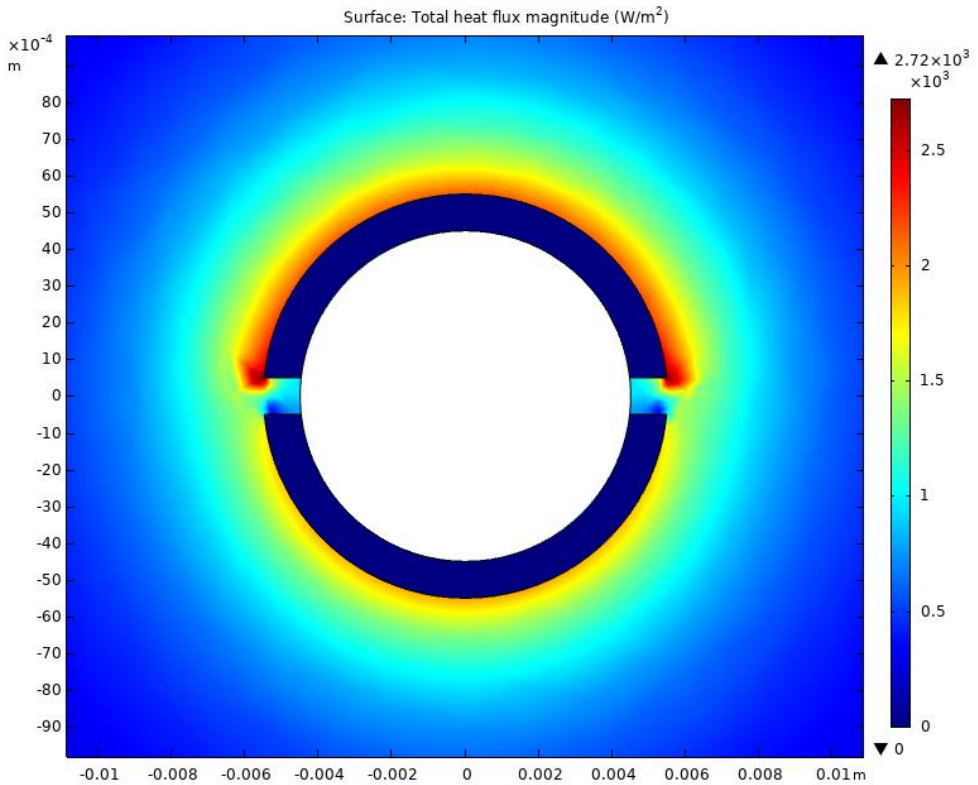

Figure 21. Heat flux distribution in the regolith body. It can be seen that upper sector's heat flux is higher and it increases a lot more near corners.

When the thermal conductivity of the regolith body is changed, a change in thermal resistance between sectors is also expected to vary. For this simulation, regolith conductivity values are picked from the range 0.1 W/mK to 5 W/mK by increasing 0.1 W/mK in every step.

$$\boldsymbol{Thermal\ Resistivity} = \frac{\mathbf{1}}{\boldsymbol{Thermal\ Conductivity}}$$

Equation 1. Relation between thermal resistivity and thermal conductivity

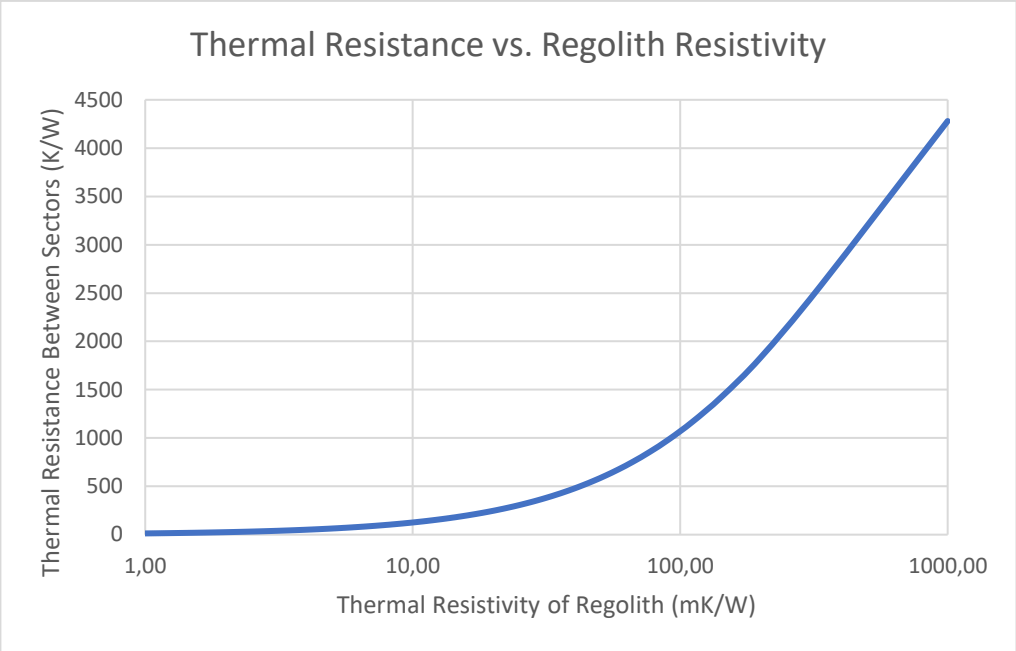

Figure 22. Thermal Resistance between upper and lower sectors as a function of thermal resistivity of the regolith body, in logarithmic scale. Here, axis value of 1000 mK/W means 0.001 W/mK of thermal conductivity of regolith where the thermal resistance values rise quickly around that number.

This graph shows that, when the resistivity of the regolith body to heat transfer increases, the resistance between sectors also increases. In other words, the difficult it becomes for the regolith to transfer heat, the closer the value of total heat flux' of the sectors become.

4.1.2.2. Thermal Resistance Calculations for Four Sectors

Previous settings for two sector simulation are preserved and sensor is redesigned so that it would have four sectors with equal areas.

Dimensions of the regolith body is increased to 0.7 x 0.7 x 0.7 m which helped the temperature to be more homogeneous especially at the top and bottom surfaces.

The inside material of the sensor sphere is disabled, which was previously air and different temperature values for sectors are tried (providing 1 K difference) to obtain more concrete results.

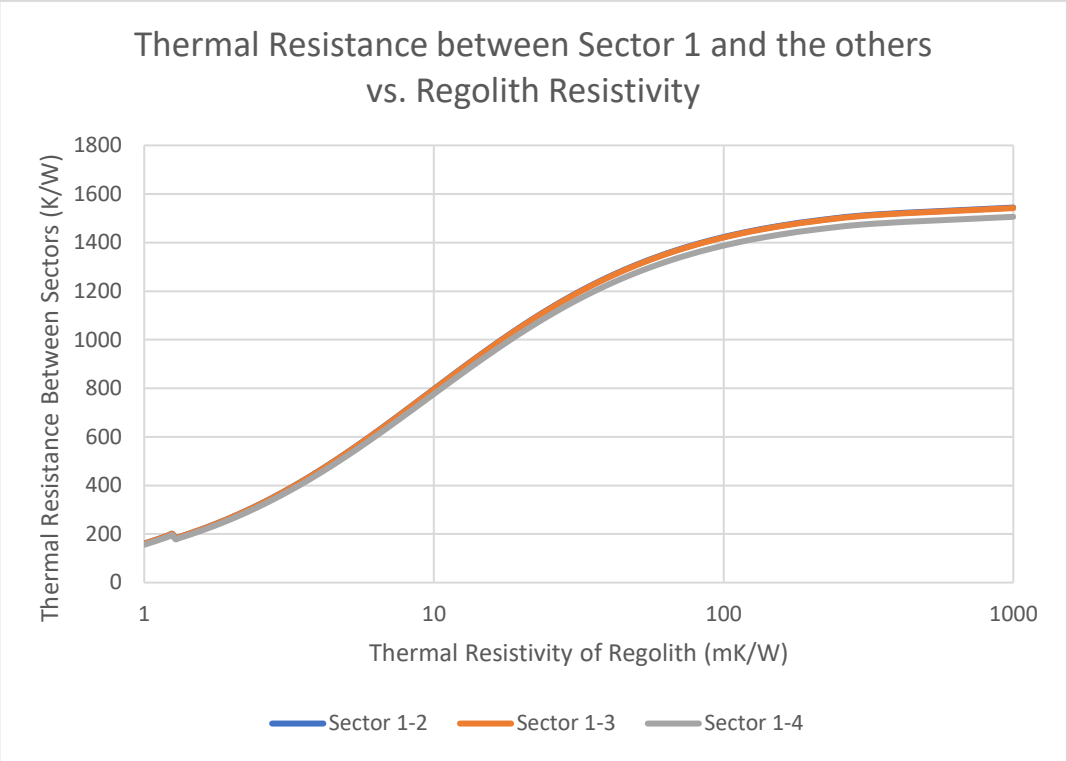

Figure 23. Thermal Resistance between sector 1 and the other sectors.

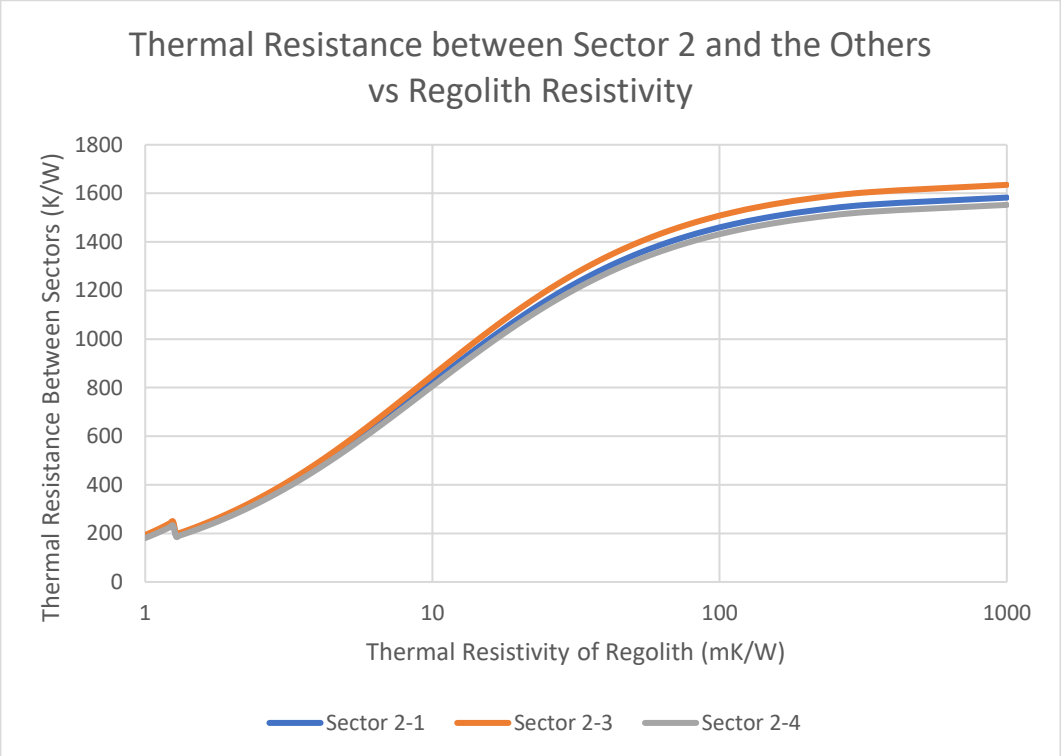

Figure 24. Thermal Resistance between sector 2 and the other sectors.

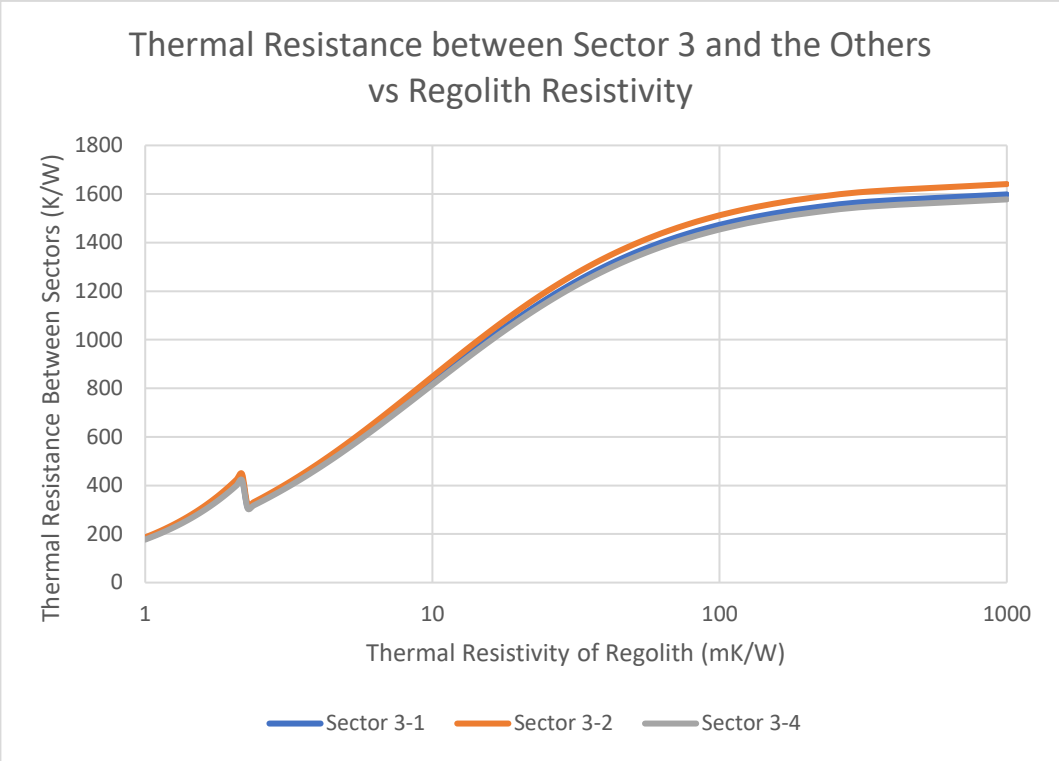

Figure 25. Thermal Resistance between sector 3 and the other sectors.

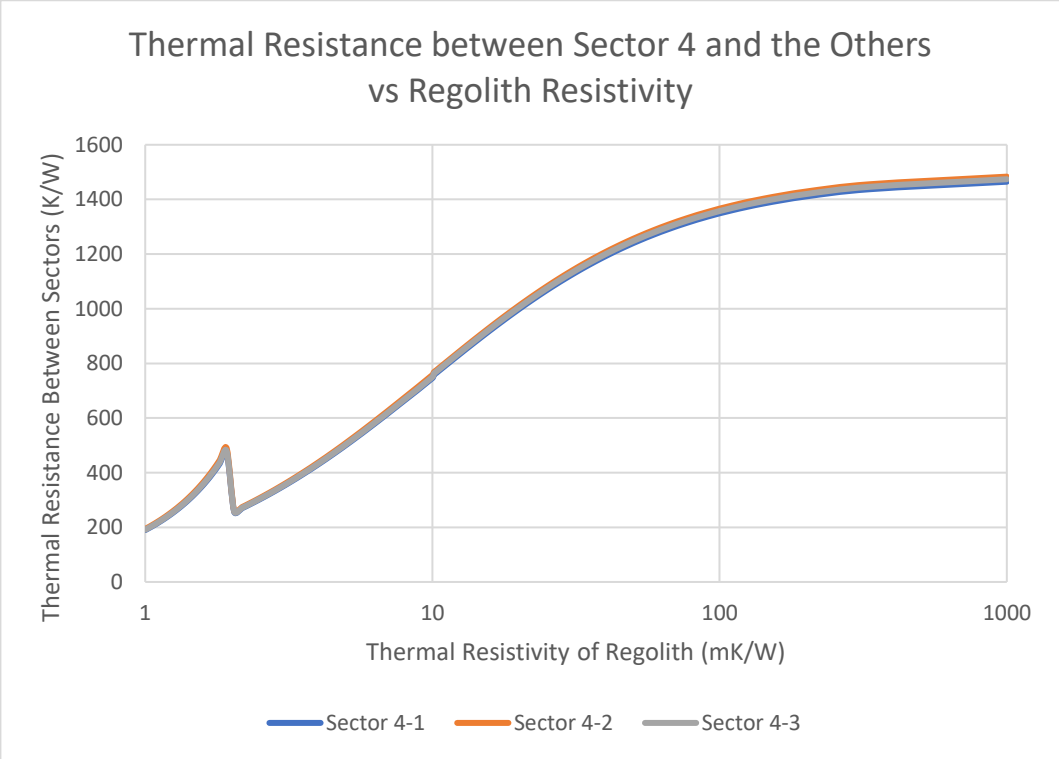

Figure 26. Thermal Resistance between sector 4 and the other sectors.

One of the important aspects to understand here is that there is a symmetry between sectors, therefore their thermal resistance values are identical.

Boundary conditions are set as all 6 walls of the setup are adiabatic, where the heat flux on the walls are equal to zero.

Small anomalies between 1 and 10 mK/W is supposed to be an artifact of the simulation program.

The lesson we can learn from here can be, when the regolith body becomes enormously resistive to the heat transfer, the thermal resistance between sectors converge at a specific value, which is around 1600 K/W.

4.2. Calculations for the Thermal Impedance & Phase Difference as a function of Frequency

Impedance definition in electrical engineering originally indicates the current opposition of a circuit when a voltage is applied to it. It is a function of resistance, capacitance and inductance. This phenomenon naturally needs an electrical environment to be mentioned. Frequency is also an electrical term in Hz, indicating the number of a repeating event in a certain unit of time.

If these elements are wanted to be observed in a different environment, the challenge here would be to express and apply these electrical terms successfully into a thermodynamic setting.

To start with impedance, this term can be applied into a non-electrical habitat by shifting definitions to interdisciplinary ones.

Thermal impedance becomes basically thermal resistance in the discipline of thermodynamics, unlike the difference between electrical resistance and electrical impedance. As thermal conductance is watt per kelvins (W/K), thermal resistance becomes kelvins per watt (K/W).

On the other hand, frequency would be harder to implement, a way must be found to apply a recurring event in thermodynamics.

Changing the temperature on the surface of the sphere is selected as a frequency term after further considerations. To do this, temperature is changed with respect to time, using a sinusoidal function. This sinusoidal function has a basis of sphere temperature and varies from -30 K to +30 K.

The equation of mentioned sinusoidal function is as following:

$$T_{sphere} = T_{bottom} + 30\ sin\left(\frac{t\frac{180}{\pi}}{timepar}\right)$$

Equation 2. Function used to change the temperature of the surface of the sphere with time.

Here, 'timepar' parameter is just used to ensure the unit consistency inside software.

In this setup, the environment changes to Martian air which is CO2 rich. An air input and output are provided with a certain wind speed. To do this, Multiphysics tool is used in COMSOL. First, a non-isothermal flow is defined. Inside this physics model, fluid volume is defined and initial values (pressure and temperature) are selected. After inlet and outlet areas are selected, inlet wind and outlet pressures are defined. Finally, constant temperature values for inlet, outlet and sphere areas are designated. Also, boundary conditions for heat transfer is defined on walls and on sensor body, which indicate a thermal insulation.

To obtain the thermal impedance, two outputs must be collected; total normal heat flux dissipating from the sphere, and the temperature of the sphere. These data are both have a sinusoidal output. Desired information here would be their amplitude. Therefore, minimum and maximum values of these two are taken and subtracted from each other. At the end, thermal impedance would be the ratio of temperature's amplitude to the heat flux's amplitude. With this procedure, one definite thermal impedance value can be obtained from two varying sinusoidal curves. [4]

$$Thermal\ Impedance\ (K/W) = \frac{Sensor\ Temperature_{max} - Sensor\ Temperature_{min}}{Total\ Sensor\ Heat\ Flux_{max} - Total\ Sensor\ Heat\ Flux_{min}}$$

Equation 3. Equation to obtain thermal impedance. Denominator and dividend indicating the amplitudes, while the overall division ensures the unit consistency for thermal impedance.

Again, this simulation can be performed with different frequency values. One should remember that temperature dependent frequency changes are much slower than electrical frequency changes. So, high frequencies above 5 Hz can create an inconsistency in results.

It would be an interesting point of view to observe thermal impedance as a function of frequency. Moreover, different wind speed values passing through the funnel can be tried to understand the characteristic of the thermal impedance. Below graph shows this approach with two different wind speeds.

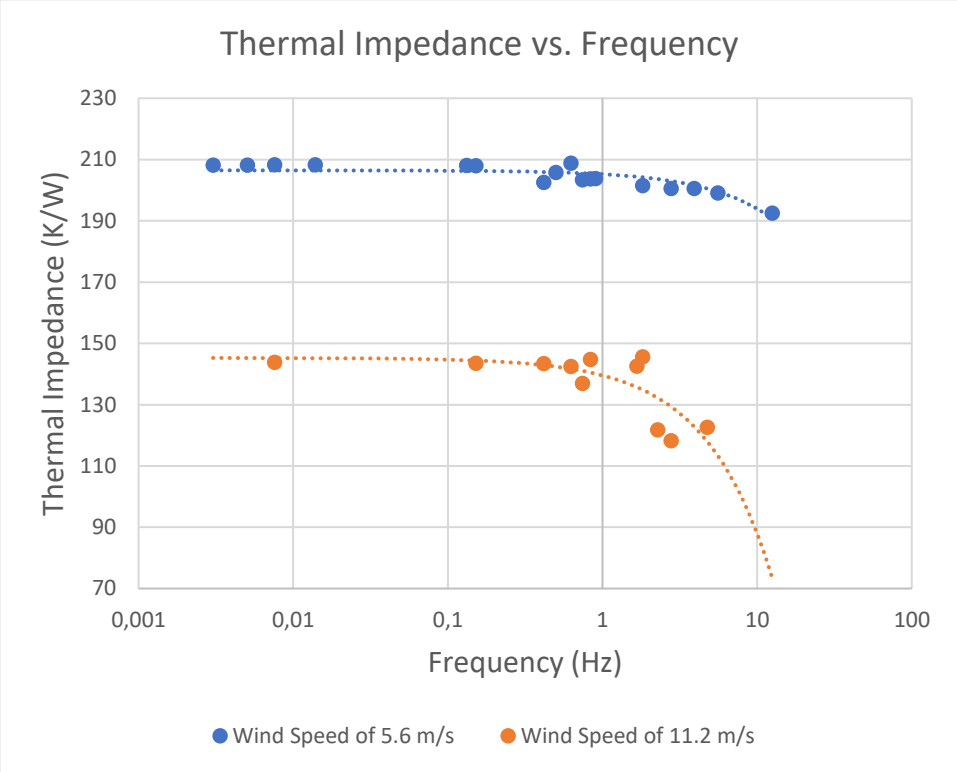

Figure 27. Thermal impedance as a function of thermal frequency (in logarithmic scale). Wind speed of 5.6 m/s and 11.2 m/s are used to get different curves.

This new result about the sensor indicates some interesting lessons. When thermal frequency increases, which indicates how fast the temperature of the sphere changes, the real part of the thermal impedance starts to decrease. This real part also refers to the thermal resistance. Besides, it decreases when the speed of the wind increases.

In addition, this decrease in impedance swell with the increased wind speed. In other words, thermal impedance value as a function of frequency, decreases faster with increased wind speed. One should remember that the frequency axis is logarithmic.

In electrical definition, impedance has two elements: a real part and an imaginary part. The thermal impedance which is calculated above is the real part of it. The second element, imaginary part consists of a phase angle between current and the voltage. In our setup, this phase difference indicates the angle between two different sinusoidal functions which are the temperature of the sphere and the heat flux of the sphere changing with time. It is easy to foresee that there will be a delay on the heat flux dissipated when sphere's

temperature is changed. Simply, this time delay gives the phase difference of the thermal impedance.

After obtaining sinusoidal functions, this angle can be measured manually. The graph below shows this phase difference as a function of frequency using again two different wind speeds.

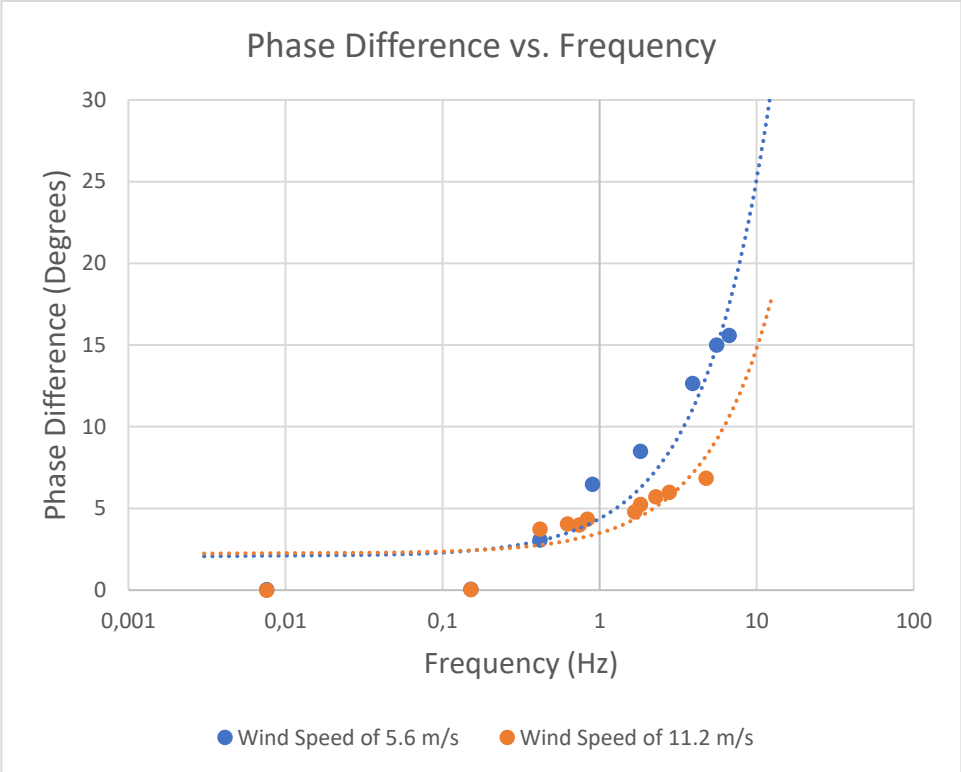

Figure 28. Phase difference as a function of thermal frequency. Wind speed of 5.6 m/s and 11.2 m/s are used to get different curves.

This graph shows that the phase difference between temperature and heat flux sinusoidal waves increases with frequency. There is a correlation between wind speed and the exponentiality of the phase difference increase. The faster wind passes from the tunnel, the slower the phase difference increases with frequency.

Small frequencies create extremely low phase differences, but after 1 Hz, radical increases can be seen.

Furthermore, to support these, some of the graphs used to obtain these data are shown below. One should remember that the more frequency increases, the fragile the simulations become. It is seen that an instability occurs above a frequency value of approximately 5 Hz. This might happen because of the decreased step size for high frequencies. Very small

step sizes are unwanted in the simulation program COMSOL. This instable situation manifest itself stronger also when high wind speeds are used.

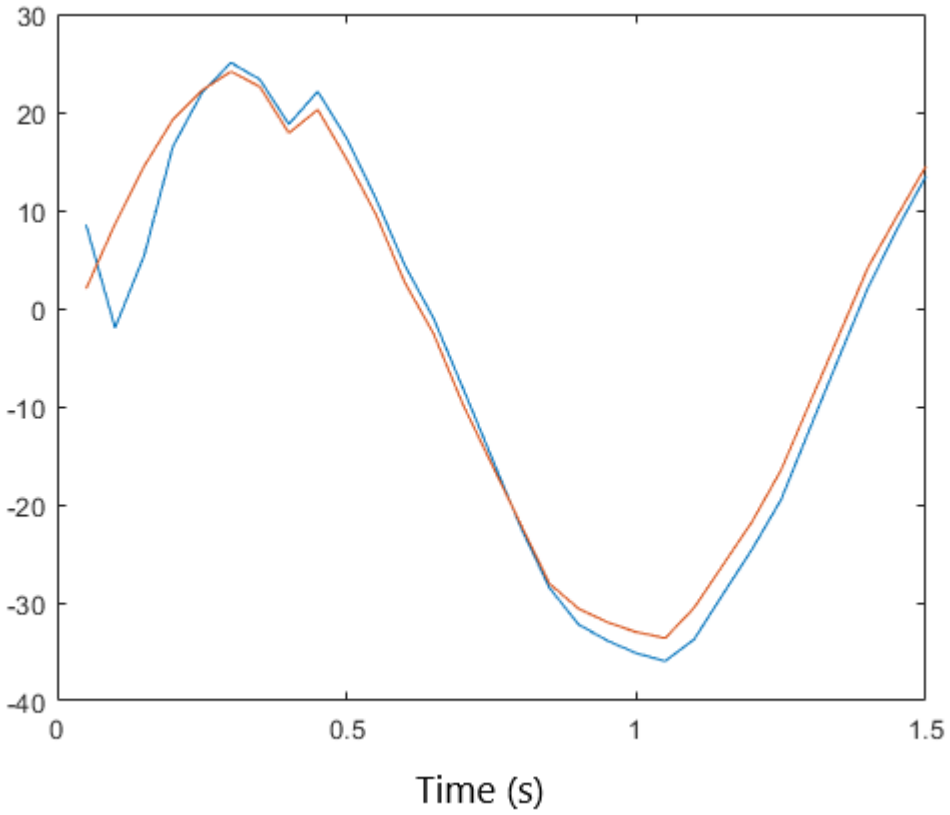

Figure 29. Above graph shows two lines, red one indicating temperature change with time, and the blue one indicating heat flux change on the surface where temperature fluctuates. While x-axis represents time in seconds, y-axis represents unitless values. The frequency is measured as 0.741 Hz. Wind speed for this case is 11.2 m/s.

To see the overlapping clearly, each graph is first subtracted from a reference point. Then, multiplied by a value to equalise both of them. The space between the graphs present us the time difference between them, which leads to the angle difference:

$$Phase\ Difference\ (°) = Time\ Difference * 360 * Frequency$$

Equation 4. Formula used to obtain phase difference using the time difference between graphs

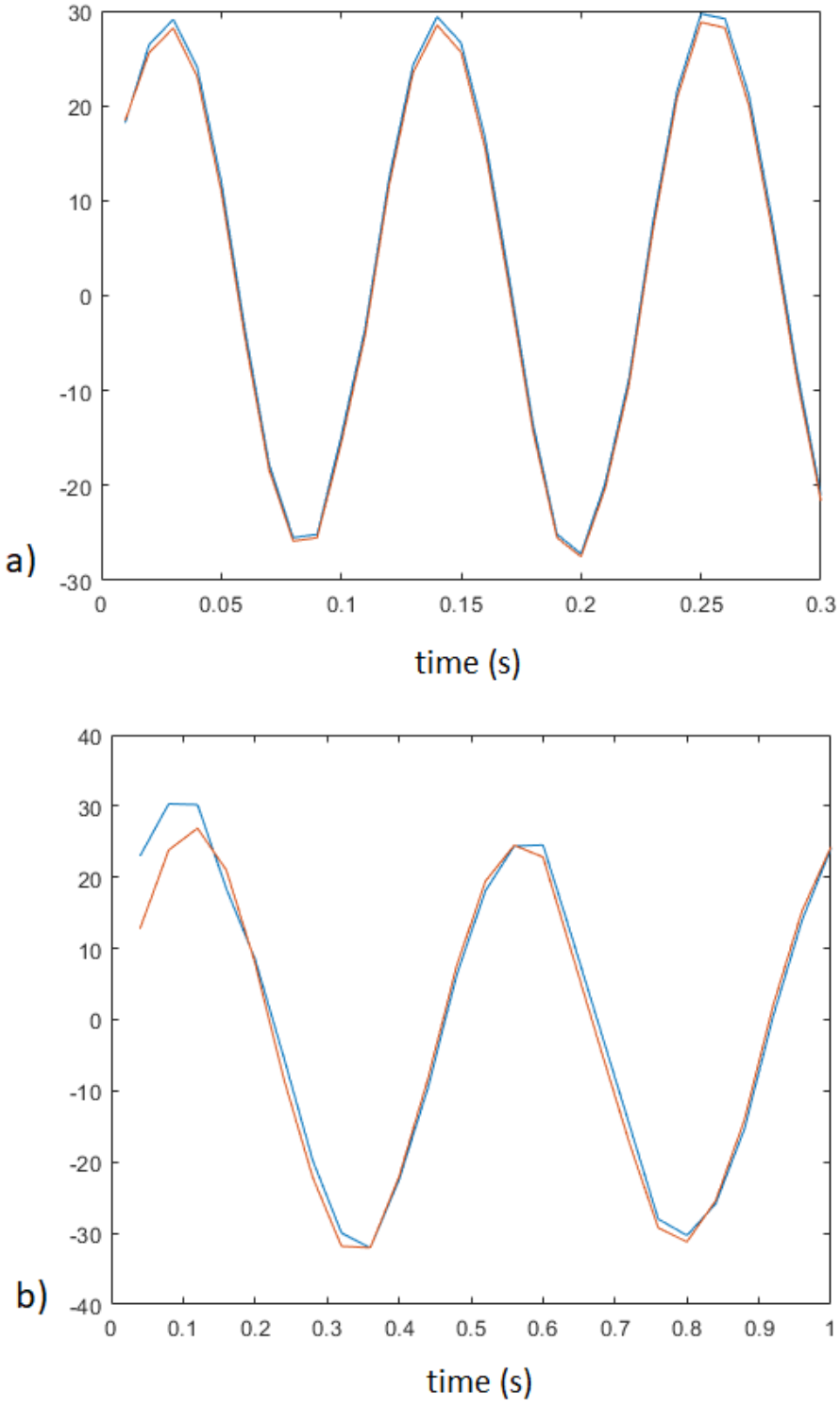

Figure 30. Another example for thermal impedance measurements. Two different frequencies are included here to help see the phase difference. In the uppermost figure, it is nearly impossible to realise a phase difference with naked eyes. One can see the slightly increased phase difference as frequency increases below: a) 0.1515 Hz with 11.2 m/s wind speed. b) 2.2727 Hz with 11.2 m/s wind speed.

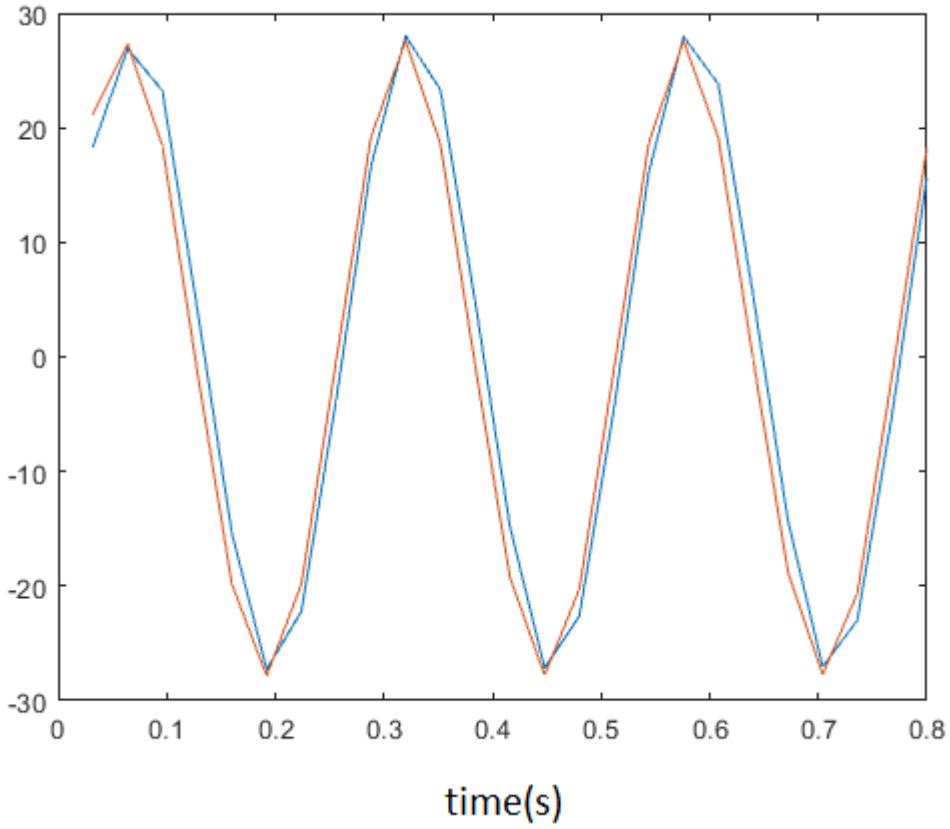

Figure 31. A wind speed of 5.6 m/s is used for this graph while frequency is measured as 3.90 Hz. It is mentioned that decreased wind speed and higher frequencies lead to higher phase differences. In this graph, this phenomenon can be seen as phase difference is much larger with respect to previous ones.

5. Budget

In this study, only computational costs may be counted. It is estimated that more than 200 discrete simulations are performed which means over 4000 minutes of computation.

For this, personal computer as well as university's are used.

6. Conclusions and future development

This research aimed to find the answers of previously described objectives about a newly introduced 3D heat flow sensor. Based on the quantitative analysis performed, the answers can be clearly stated.

1. The study started with investigating the impact of the plastic film covering the 3D heat flow sensor for the protection. The power signal from the sensor is observed and it is seen that the plastic film has an obvious impact, slightly increasing the amplitude of the power signal.
2. The investigation of the relation between thermal resistance of the two sectors and the thermal resistivity of the regolith taught the lesson that, the difficult it becomes for the regolith to transfer heat, the closer the value of total heat flux' of the sectors become. Increased resistivity of the regolith leads sectors to have similar heat flux values.

   This idea does not change when four-sector-sensor is applied. A major appearance emerged that, with astronomical resistivity values, thermal resistances of the sectors converge to a specific number around 1600 K/W. Plus, a symmetry is observed between sectors.
3. Thermal impedance has a relation with the thermal frequency. As frequency term here is described as the change of the temperature on the sensor, results become interesting to comment on. When thermal frequency increases, it is observed that impedance decreases. But this decline's slope increases when the wind speed is increased. Moreover, wind speed does not only affect this slope. It also affects the value of thermal impedance. When wind speed increases, thermal impedance values decrease significantly when compared to higher wind speeds.
4. Finally, it is necessary to examine the result for the phase difference between temperature and heat flux waves. This angle difference clearly increases with frequency. The faster temperature changes on the sensor sphere, the difficult it becomes for the heat flux wave to catch the temperature wave.

   A correlation can be seen between wind speed and the increase of the phase difference. Higher wind speeds prevent the angle difference to increase. Therefore, with lower wind speeds, phase difference increases more exponentially.

This research presented new series of numerical analysis for a new 3D heat flow sensor. The expectations for this analysis are mostly met with the reality and foresight. One misfortune that nobody could foresee was the pandemic which affected the direction of the

work and also limited possible opportunities. But in other respects, the results still demonstrate a huge potentiality.

To better see the implications of these results, future studies could address a better understanding of this novel sensor and its great potential for space exploration. Future is certainly relying on planetary exploration and humanity will see this new born reality in upcoming years and raise his attention much closer.

Bibliography

[1] Kowalski, L., Atienza, M. T., Gorreta, S., Jimenez, V., Dominguez-Pumar, M., Silvestre, S., & Castaner, L. M. (2016). *Spherical Wind Sensor for the Atmosphere of Mars. IEEE Sensors Journal, 16(7), 1887–1897.* doi:10.1109/jsen.2015.2509168

[2] https://mars.nasa.gov/msl/spacecraft/instruments/rems/

[3] Domínguez-Pumar, M., Rodríguez-Manfredi, J.-A., Jiménez, V., Bermejo, S., & Pons-Nin, J. (2020). *A Miniaturized 3D Heat Flux Sensor to Characterize Heat Transfer in Regolith of Planets and Small Bodies. Sensors, 20(15), 4135.* doi:10.3390/s20154135

[4] Lagha, H., Chazal, H., & Belmabrouk, H. (2014). A new approach for generating compact thermal models. 2014 International Conference on Electrical Sciences and Technologies in Maghreb (CISTEM). doi:10.1109/cistem.2014.7076976

[5] Carmona, M., Marco, S., Palacin, J., & Samitier, J. (1999). *A time-domain method for the analysis of thermal impedance response preserving the convolution form. IEEE Transactions on Components and Packaging Technologies, 22(2), 238–244.* doi:10.1109/6144.774738

[6] Ma, K., He, N., Liserre, M., & Blaabjerg, F. (2016). Frequency-Domain Thermal Modeling and Characterization of Power Semiconductor Devices. IEEE Transactions on Power Electronics, 31(10), 7183–7193. doi:10.1109/tpel.2015.2509506

[7] Mora-Ventura, B., Eder Sánchez, J., González, G., & González, F. J. (2020). *Thermal Impedance Analysis of Nano-Dipole Linear Arrays for Energy Harvesting Applications. Infrared Physics & Technology, 103332.* doi:10.1016/j.infrared.2020.103332